Soil & Tillage Research 213 (2021) 105159

Contents lists available at ScienceDirect

Soil & Tillage Research

journal homepage: www.elsevier.com/locate/still

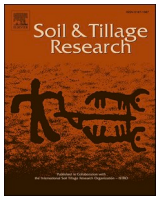

# Soil detachment capacity by rill flow for five typical loess soils on the Loess Plateau of China

Nan Shen [a,b], Zhanli Wang [a,b,*], Qi Guo [b,c], Qingwei Zhang [d], Bing Wu [e], June Liu [f], Chunyan Ma [g], Claudio O. Delang [h], Fengbao Zhang [a,b,*]

[a] State Key Laboratory of Soil Erosion and Dryland Farming on the Loess Plateau, Institute of Soil and Water Conservation, Northwest A&F University, Yangling, Shaanxi, 712100, China
[b] State Key Laboratory of Soil Erosion and Dryland Farming on the Loess Plateau, Institute of Soil and Water Conservation, Chinese Academy of Sciences and Ministry of Water Resources, Yangling, Shaanxi, 712100, China
[c] University of Chinese Academy of Sciences, Beijing, 100049, China
[d] School of Resources and Environment, Northwest A&F University, Yangling, Shaanxi, 712100, China
[e] Department of Civil Engineering, School of Human Settlements and Civil Engineering, Xi'an Jiaotong University, Xi'an, Shaanxi, 710049, China
[f] School of Geography and Tourism, Shaanxi Normal University, Xi'an, Shaanxi, 710119, China
[g] College of Life Sciences, Yulin University, Yuling, Shaanxi, 719000, China
[h] Department of Geography Hong Kong Baptist University, Kowloon Tong, Hong Kong, 999077, China

ARTICLE INFO

*Keywords:*
The loess plateau
Rill erosion
Soil detachment capacity
Effective soil particle size
Soil cohesion
Stream power

ABSTRACT

The loess region of China is one of the most heavily eroded areas in the world. Soil detachment capacity by rill flow ($D_c$) is a key parameter for quantifying intensity of rill erosion in many process-based erosion models. However, only a limited number of studies have been devoted to soil detachment capacity for the various types of loess soil such as is found on the Loess Plateau, where there is variation from south to north and in terms of soil particle size composition. The objectives of this study were (1) to discriminate differences in soil detachment capacity by rill flow ($D_c$) among five loess soils, (2) to investigate the relationship between $D_c$ and hydrodynamic parameters, and the relationship between $D_c$ and soil properties, and (3) to establish an equation to model soil detachment capacity by rill flow for the loess region. Soil detachment capacity by rill flow for five typical loess soils found on the Loess Plateau of China was investigated through a flume experiment by varying five flow discharges and five slope gradients. The results show that $D_c$ of SM sandy loess is the largest with a mean of 2.2145 kg $m^{-2}$ $s^{-1}$, followed by YL clay loess, DB sandy loess, AS loess, and CW loess. Stream power is the best hydrodynamic parameter to describe the dynamic process of soil detachment capacity by rill flow for these five loess soils. Soil detachment capacity by rill flow was negatively correlated with soil cohesion and effective silt content ($P < 0.05$), while it was positively correlated with effective median soil particle size ($P < 0.01$) and effective sand content ($P < 0.05$). Soil detachment capacity by rill flow for various hydraulic and soil conditions in the loess region could be modeled using a quaternary power function of slope gradient, flow discharge, soil cohesion and effective median particle size ($NSE = 0.96$), or it could be modeled by a ternary power function which calculates the variation of soil detachment capacity with stream power, soil cohesion and effective median size ($NSE = 0.96$). The results of this study reveal the mechanism of soil detachment by rill flow and advance development of a physically-based rill erosion model. Future research should focus on the impact of effective particle size on $D_c$ to ensure a full understanding of soil erosion processes.

## 1. Introduction

Soil detachment by rill flow, sediment transport and deposition of soil particles are the three processes of rill erosion. Soil detachment by rill flow is the initial process, providing sediment for rill flow during transport and changing clear rill flow into sediment-laden. Soil detachment capacity by rill flow ($D_c$) is defined as the maximum soil detachment rate for clear rill flow. $D_c$ has an restriction on the process of

* Corresponding authors at: State Key Laboratory of Soil Erosion and Dryland Farming on the Loess Plateau, Institute of Soil and Water Conservation, Northwest A&F University, Yangling, Shaanxi, 712100, China.
*E-mail addresses:* zwang@nwsuaf.edu.cn (Z. Wang), fbzhang@nwsuaf.edu.cn (F. Zhang).

https://doi.org/10.1016/j.still.2021.105159
Received 6 February 2021; Received in revised form 3 June 2021; Accepted 30 July 2021
Available online 5 August 2021

soil detachment and is a key parameter for quantifying the intensity of soil detachment. In the well-known physically-based WEPP (Water Erosion Prediction Project) model, soil detachment capacity is used as one of the control parameters in the governing equation for rill erosion (Flangan and Nearing, 1995). The comprehensive study and accurate estimation of soil detachment capacity by rill flow is a necessary prerequisite to reveal the process of rill erosion, to develop a rill erosion model based on physical processes, and finally to accurately predict rill erosion intensity.

Soil detachment capacity by rill flow is mainly controlled by the hydrodynamic characteristics of rill flow and soil properties on the hillslope (Gover, 1992; Liu et al., 2016; Li et al., 2015a; Mamo and Bubenzer, 2001; Nearing et al., 1991, 1997a; Sun et al., 2014; Zhang et al., 2002, 2003). Flow shear stress, stream power and unit stream power are commonly used hydrodynamic parameters to characterize flow dynamics. These parameters reflect the hydraulic characteristics of rill flow from the perspectives of force and energy. It is essential to explore the relationship between soil detachment capacity by rill flow and hydrodynamic parameters and to determine the optimal parameters that reveal the dynamic mechanism of soil detachment by rill flow.

Gimenez and Govers (2002) evaluated soil detachment by concentrated flow on smooth and rough beds. Their results showed that shear stress is the most universal detachment predictor in rills. The same result was confirmed by Cao et al. (2011) in their study of soil detachment on unpaved road surfaces by flowing water. The physical equations for soil detachment by simulated concentrated flow predicted by Wang et al. (2012) illustrated that the detachment rate is linearly correlated with shear stress. But for various soils, different detachment subprocesses become dominant (Elliot and Laflen, 1993) and shear stress is not necessarily the best detachment predictor (Knapen et al., 2007). Zhang et al. (2002, 2003) studied soil detachment capacity by shallow flow and concluded that stream power was the optimal hydraulic parameter for accurately predicting the detachment rate. The advantage of stream power in predicting soil detachment was also confirmed by Nearing et al. (1999); Zhang et al. (2015); Wang et al. (2016); Xiao et al. (2017). However, Li et al. (2015a) measured soil detachment capacities under six hydraulic conditions and concluded that $D_c$ increased as a power function of either shear stress or stream power with a coefficient of determination of 0.42. This result is inconsistent with the conclusions of previous studies that stream power was better than shear stress for simulating the soil detachment process (Nearing et al., 1999; Zhang et al., 2003). In addition to shear stress and stream power, unit stream power also has been used as a hydrodynamic parameter to model the process of soil erosion. In the soil erosion models EUROSEM and LISEM, the soil detachment rate is expressed by sediment transport capacity and sediment settlement rate, in which sediment transport capacity is computed based on unit stream power (Misra and Rose, 1996; De Roo et al., 1996; Morgan et al., 1998; Govers, 1990). Ali et al. (2013) established a sediment transport function based on unit discharge to predict soil erosion. However, the prediction accuracy of unit stream power for soil detachment capacity is low, thus it is a good predictor for sediment transport but not for soil detachment.

The process of soil detachment by runoff occurs in the surface layer of soil, so surface soil properties directly affect the rate of soil detachment. Soil factors affecting the detachment process include soil type, texture, bulk density, soil cohesion, organic matter content, aggregates characteristics, initial water content, etc. (Su at al. 2014; De Baets and Poesen, 2010; Ciampalini and Torri, 1998; Ghebreiyessus et al., 1994; Morgan et al., 1998; Knapen et al., 2007; Zhang et al., 2008; Wang et al., 2015, 2012; Torri et al., 1998). Li et al. (2015a) found that soil type influenced soil detachment capacity significantly. Soil detachment capacity of yellow loess soil was 1.49 times greater than that of red loess soil. Su at al. (2014) quantified the effects of soil type on detachment capacity using soil samples collected from the Beijing Region of China. Their results showed that soil detachment capacities were significantly affected by soil type. De Baets and Poesen (2010) found that bulk density and soil moisture could be used to estimate $D_c$. Zhang et al. (2008) found that the soil detachment capacity was closely related to soil clay content, bulk density, median diameter of aggregates and soil cohesion. Ciampalini and Torri (1998) constructed a flume to measure detachment rate of soil particles by shallow flow. Their results showed that variations in initial soil moisture conditions and soil surface characteristics caused differences in soil detachment capacity by overland flow.

Land use, plant roots, and biological crusts affect surface soil moisture, organic matter, bulk density, soil cohesion and other soil properties, thus influencing the process of soil detachment (Liu et al., 2019; Wang et al., 2013; Li et al., 2015a; Zhang et al., 2008; De Baets et al., 2006. Li et al. (2015a) proposed that the variability of $D_c$ under different land uses was positively related to silt content, and inversely related to sand content, cohesion, water stable aggregate, aggregate median diameter, organic matter, and root density. Similar results were found by De Baets et al. (2006), that soil detachment during concentrated flow over grass roots compared to bare conditions showed an exponential decay function with increasing root density. Wang et al. (2013) used flow shear stress and biological crust thickness to simulate soil detachment capacities by a power function for abandoned farmland. Geng et al. (2021) recently studied the response of soil detachment capacity to landscape position and found that soil organic matter, water stable aggregate, root mass density, and soil cohesion dominated the variations in $D_c$. For six landscape positions, $D_c$ was estimated satisfactorily by stream power, water stable aggregate and root mass density with $R^2$ of 0.81.

The Loess Plateau of China is the largest loess region and the most heavily eroded area in the world. It is covered with a thick layer of highly erodible aeolian silt deposits, which are loose, porous, fine, and rich in vertical fissures (Zheng et al., 2020). The severe soil erosion in this region has caused serious threats to local sustainable development and the safety of the lower reaches of the Yellow River. Rill erosion is one of the most important soil erosion types and a source of sediment yield in the Loess Plateau. Study of the soil detachment capacity by rill flow on the Loess Plateau can reveal the rill erosion process mechanism for this region, scientifically establish the rill erosion process model, and provide a theoretical basis for soil erosion control and ecological construction on the Loess Plateau. Many studies have tackled the problem of soil detachment capacity in association with flow hydraulics, soil properties and other factors. However, only a limited number of studies have been devoted to soil detachment capacity for various soil types, especially for soil types which reflect the variation from south to north on the Loess Plateau and differences in soil particle size composition from fine to coarse. Moreover, there have been limited studies of soil detachment capacity using a non-erodible bed inset with a small soil sample for detachment measurement. This design can measure soil detachment capacity accurately and avoid the influence caused by the occurrence of deposition, because it ensures that the maximum detachment rate of soil samples by clean water can be measured by eliminating the sediment feedback effect caused by increased sediment load in rill flow and deposition of soil particles.

In this study, five types of loess soil from the Loess Plateau were selected as test soils for the flume experiment conducted using the non-erodible bed and small inset soil sample design. The main objectives of this study were (1) to discriminate between differences in soil detachment capacity by rill flow ($D_c$) among five loess soils, (2) to investigate the key hydrodynamic factors and key soil properties factors influencing $D_c$, and (3) to establish an equation to model soil detachment capacity by rill flow for the loess region using affecting factors.

## 2. Materials and methods

### 2.1. Study area and test soil

The Loess Plateau, located in the northern part of central China, is the largest loess region on Earth. Academician Liu (1966) pointed out in

his book *Material Composition and Structure of Loess* that the particle size of loess on the Loess Plateau gradually becomes coarser from southeast to northwest, and delineated horizontal zones of loess in the Loess Plateau region according to the content of sand and clay (Fig 1). According to the zoning map, loess distribution on the Loess Plateau can be divided into three zones, namely, the clay loess zone, the loess zone, and the sandy loess zone. Therefore, five types of loess soil were collected as test soil for this study to capture variations in loess based on geographical location from south to north and soil particle size composition from fine to coarse. The sampling sites were located in Yangling (34°14′ N, 107°59′ E), Changwu (35°18′N, 107°38′ E), Ansai (36°30′ N, 109°26′ E), Dingbian (37°53′ N, 108°22′ E) and Shenmu (38°46 N, 110°21′ E), as shown in Fig. 1. The five test soils are YL clay loess, CW loess, AS loess, DB sandy loess, and SM sandy loess. The depth of soil collection was 30 cm. The land use was farmland. The basic properties of the tested soils are shown in Table 1. According to the USDA classification, the soil textures were silty clay loam, silty loam, loam, and sandy loam.

### 2.2. Experimental devices and designs

A rill flume (PVC plate) 4 m long, 0.1 m wide, and 0.1 m deep was used to measure soil detachment capacity, as shown in Fig. 2. The flume length of 4 m was designed mainly based on the summary of previous researches that conducted flume experiment and the concern of material costs. The shape of rill flume is rectangular. A layer of test soil was uniformly bonded using paint to the bed of the flume to simulate the roughness of a natural soil surface. The bed of the flume was polished to remove the soil previously bonded to it once the experiment for that type of soil was finished, then the next test soil was bonded. The slope of the flume could be adjusted within the slope range of 5°~25 ° by manually adjusting the lifting device at the end of the flume. Flow discharge was controlled by a flow meter and was calibrated before each measurement of $D_c$. A square hole just large enough to fit the soil sample box sized 0.1 m by 0.1 cm by 0.05 cm was arranged at the outlet end of the flume. The top surface of the soil sample in the sample box was placed flush with the flume bed. A slip lid was placed over the sample box to control the process of soil detachment by rill flow before measurement.

The five test soils were screened with a 5mm-sieve to filter out grass roots, stone particles and other impurities. Then the water content of the test soils was measured. The test soils were naturally dried to a 14 % water content if the measured water content was higher than 14 %, and water was added using a spray bottle if the water content was lower than 14 %. Soil that had been sprayed with water was placed in a sealed plastic bucket for 48 h to further balance the soil water. Once the correct water content was obtained, the soil was weighed and packed into a soil sample box in two 2.5 cm-thick layers to the designed bulk density indicated by in situ survey from the field (see Table 1 for details of the designed bulk density). The bottom of the soil sample box includes six small holes to ensure that it has permeability, and a piece of gauze was placed at the bottom of each soil sample box before packing the soil to prevent soil from blocking the holes. Finally, the packed soil sample boxes were placed into a large plastic box for water absorption and saturation for 12 h.

Each combination of the five slope gradients, 15.84 % (9 °), 21.26 % (12 °), 26.79 % (15 °), 32.49 % (18 °), and 38.39 % (21 °), five unit flow discharges, 0.00156 $m^2\ s^{-1}$(560 L $h^{-1}$), 0.00200 $m^2\ s^{-1}$ (720 L $h^{-1}$), 0.00244 $m^2\ s^{-1}$ (880 L $h^{-1}$), 0.00289 $m^2\ s^{-1}$ (1040 L $h^{-1}$), and 0.00333 $m^2\ s^{-1}$ (1200 L $h^{-1}$), and the five types of loess soils were tested, with each combination repeated three times. A total of 375 trials were carried out.

### 2.3. Hydraulic parameter measurement

The velocity of rill flow was measured under 25 hydraulic conditions (combination of 5 slope angles and 5 flow discharges). Velocity was measured using the dye method, by recording the time required for the stained water to flow from 2 m above the front end of the soil sample box. Velocity was measured in 3 locations: 1.0 cm away from the left and right side walls of the rill, and in the middle of the rill. Measurements in each of the locations was repeated for 3 times for a total of 9 velocity measurements, which were averaged to obtain the surface flow surface velocity. At the same time, using the monitored flow temperature, the Reynolds number was calculated and the flow pattern of rill flow was categorized. The surface velocity was multiplied by 0.6 (laminar flow), 0.7 (transitional flow) and 0.8 (turbulent flow) to obtain the average

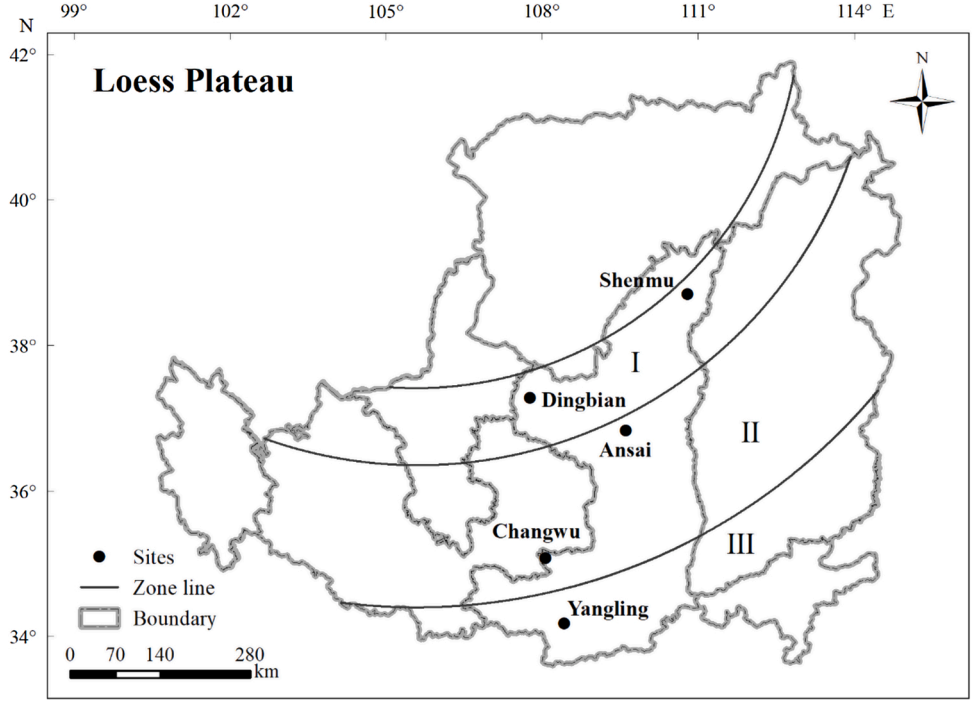


**Fig. 1.** The Loess Plateau and the location of the sampling sites (I: zone of sandy loess, II: zone of loess, III: zone of clay loess).

**Table 1**
Soil properties of the five loess soils.

| Soil | Soil code | Texture | γ | *OM* | $CaCO_3$ | *pH* | *CEC* | *CH* | Effective Particle size | | | | Ultimate particle size | | | |
|---|---|---|---|---|---|---|---|---|---|---|---|---|---|---|---|---|
| | | | | | | | | | $D_{50}$ | Clay | Silt | Sand | $D_{50}$ | Clay | Silt | Sand |
| YL clay loess | YL | Silty clay loam | 1.28 | 8.16 | 0.15 | 7.33 | 7.48 | 5.21 | 57.66 | 7.09 | 39.41 | 53.51 | 11.96 | 25.76 | 68.79 | 5.46 |
| CW loess | CW | Silty loam | 1.24 | 7.98 | 0.15 | 8.34 | 7.44 | 8.15 | 42.17 | 8.19 | 48.82 | 42.99 | 19.56 | 19.36 | 66.22 | 14.42 |
| AS loess | AS | Silty loam | 1.20 | 2.99 | 0.12 | 9.32 | 7.47 | 7.17 | 38.33 | 8.14 | 56.46 | 35.40 | 39.24 | 9.18 | 54.26 | 36.56 |
| DB sandy loess | DB | Loam | 1.23 | 3.53 | 0.11 | 9.52 | 6.90 | 5.57 | 47.64 | 8.30 | 44.31 | 47.39 | 47.47 | 8.04 | 44.97 | 47.00 |
| SM sandy loess | SM | Sandy loam | 1.36 | 1.85 | 0.07 | 9.55 | 6.66 | 4.23 | 59.81 | 4.64 | 35.31 | 60.05 | 59.03 | 5.71 | 34.84 | 59.45 |

$D_c$: soil detachment capacity by rill flow (kg $m^{-2}$ $s^{-1}$) ; γ: soil bulk density (g $cm^{-3}$); *OM*: organic matter content (g $kg^{-1}$); $CaCO_3$: calcium carbonate content (g kg); *pH : pH.*
value*; CEC*: cation substitution amount (cmol $kg^{-1}$);*CH*: soil cohesion (kPa); $D_{50}$: median particle size (μm); Clay: clay content (%); Silt: silt content (%); Sand: sand content (%).

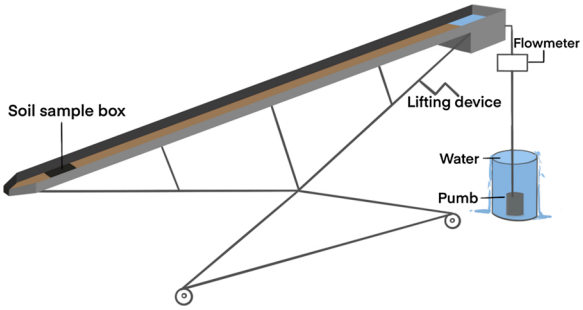


**Fig. 2.** Schematic of the rill flume.

flow velocity of rill flow layer under the combined condition of slope gradient and flow discharge (Horton et al., 1934; Luk and Merz, 1992; Zhang et al., 2002; Cao et al., 2011).

The Reynolds number, shear stress (Foster et al., 1984; Nearing et al., 1991; Cochrane and Flanagan, 1997; Zhang et al., 2009), stream power (Bagnold 1966; Misra and Rose, 1996), and unit stream power (Yang, 1972; Morgan et al., 1998; Govers et al., 2007) were calculated as follows :

$$Re = \frac{\mathrm{RV}}{v} \tag{1}$$

$$\tau = \gamma RJ \tag{2}$$

$$\omega = \tau V \tag{3}$$

$$U = VJ \tag{4}$$

where *Re* is the Reynolds number; *R* is hydraulic radius (m); *v* is viscosity coefficient of the rill flow ($cm^2$ $s^{-1}$); *τ* is flow shear stress (Pa); *ω* is stream power (W $m^{-2}$); *U* is unit stream power (m $s^{-1}$), *γ* is unit weight of water (N $m^{-3}$); *J* is hydraulic slope; *V* is flow velocity (m $s^{-1}$).

### 2.4. Soil detachment capacity by rill flow measurement

There were four steps to measure $D_c$. First, the prepared soil sample box was embedded into the square hole at the bottom of the rill flume, and the slip lid was placed to cover the soil sample. Second, the water was turned on and the flow discharge was adjusted to the designed value using a flow meter. Third, the slip lid was lifted after the flow discharge was stable and timing began. At this point the rill flow began detaching the soil sample. When the scour depth in the soil sample box reached 1.5 cm, the slip lid was placed over the soil sample and timing ended. The scour depth was kept to 1.5 cm to reduce effects from the side-wall of the soil sample box. Finally, the remaining soil in the soil sample box was carefully washed into a drying container and left for a period of time. The upper clear water was skimmed off, then the drying container was put into an oven at 105℃ for 12 h. After drying, the soil was weighed with an electronic balance, and soil detachment capacity was calculated as follows:

$$D_c = \frac{W_b - W_a}{t \times A} \tag{5}$$

where $D_c$ is soil detachment capacity by rill flow (kg $m^{-2}$ $s^{-1}$); $W_b$ is weight of the dry soil before test (kg); $W_a$ weight of the dry soil after test (kg); *t* is the duration of soil detachment (s); *A* is the projected area of soil sample ($m^2$).

### 2.5. Soil properties measurement

Soil properties were measured including bulk density, organic matter content, calcium carbonate content, soil pH value, cation exchange capacity, soil cohesion, effective soil particle size composition, and ultimate soil particle size composition. Bulk density for each soil was measured in-situ on sloping farmland. Soil organic matter content was measured through the potassium dichromate titrimetric method. Calcium carbonate content was measured using the neutralization titration gas method, while pH was measured with a pH meter. Cationic substitution amount was determined through the sodium acetate-sodium chloride exchange method. Finally, soil cohesion was measured with a 14.10 Pocket Vane Tester.

Effective soil particle size composition refers to the particle size distribution of both single particles and aggregates. For this measurement the soil sample measured with a Malvern Mastersizer 2000 laser particle size analyzer, but without treatment with a chemical dispersant. Ultimate soil particle size composition refers to the particle size distribution of single grains once aggregates have been dispersed. The soil sample was treated with a chemical for complete dispersion and then measured with the Malvern Mastersizer 2000 laser particle size analyzer. The detail process of chemical dispersion was showed below: (1) 5 g of air-dried test soil was put in a plastic cup. (2) Hydrogen peroxide was added into the plastic cup for 24 h to remove organic matter from soil.

(3) Hydrochloric acid was added to remove calcium carbonate for 24 h. (4) Distilled water was added to the upper edge of the cup for 24 h. (5) The supernatant was pour away, then 10 mL of dispersant sodium hexametaphosphate was added for two hours and the sample was test on the machine of Malvern Mastersizer 2000 laser particle size analyzer. Fig. 3 illustrates the particle size distribution of the five loess soils which was dispersed and undispersed.

In this study, the classification standard used is the USDA system that classifies clay particles as < 0.002 mm, silt particles as 0.002−0.05 mm, and sand particles as 0.05−2 mm. The measurements included effective clay content, effective silt content, effective sand content, effective median particle size, ultimate clay content, ultimate silt content, ultimate sand content and ultimate median particle size.

### 2.6. Statistical analysis

Significant differences in soil detachment capacity by rill flow among

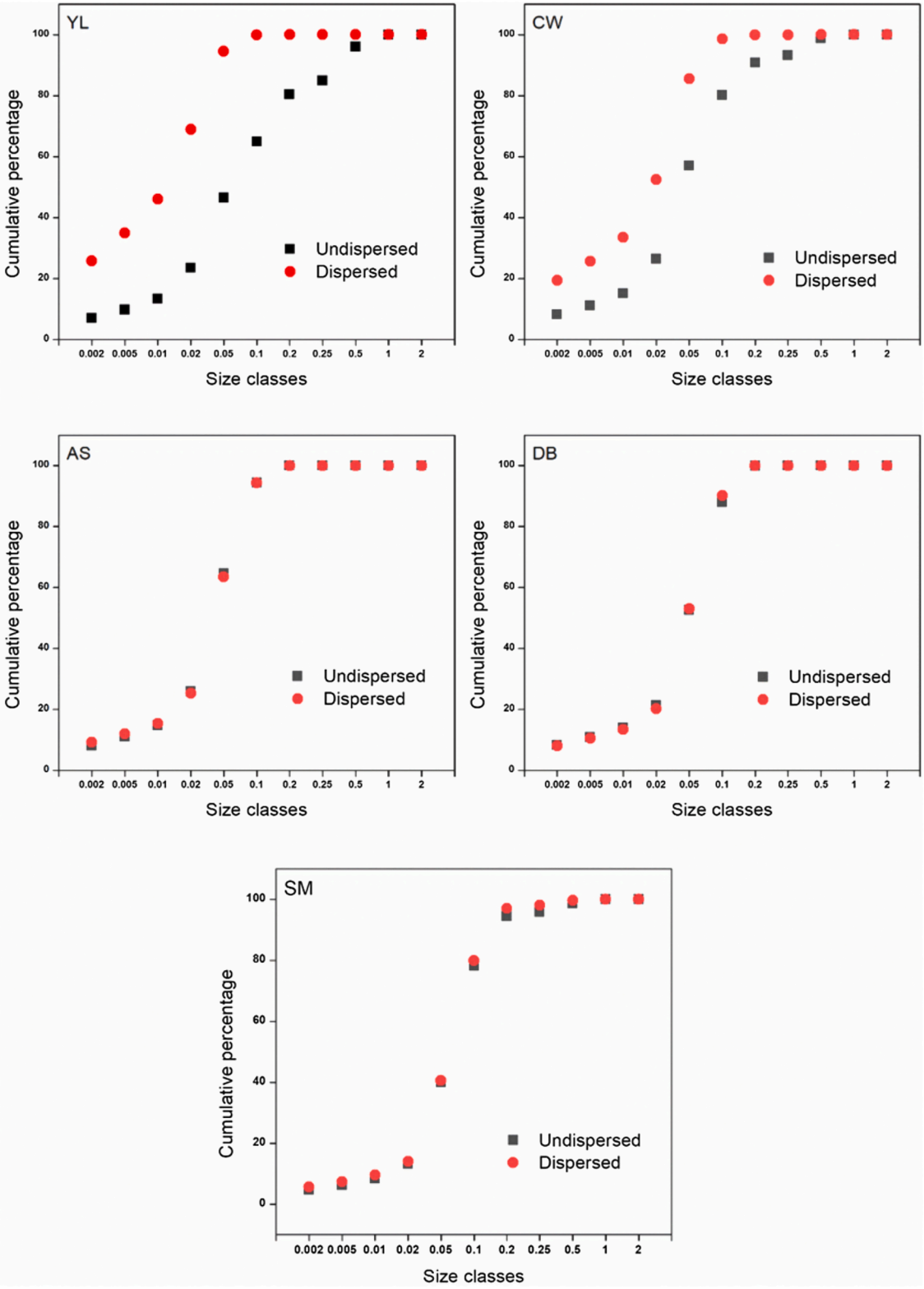


**Fig. 3.** Particle size distribution before and after being dispersed for the five loess soils (YL: YL clay loess; CW: CW loess; AS: AS loess; DB: DB sandy loess; SM: SM sandy loess).

the five soils were found using a one-way analysis of variance (ANOVA) followed by LSD ($p < 0.05$) and two-way ANOVA analysis. Relationships between $D_c$ and hydrodynamic parameters, and $D_c$ and soil properties were analyzed by simple regression. A non-linear regression method was used to model the relationships between soil detachment capacity and flow discharge, slope gradient, hydrodynamic parameters, and soil properties. Mean absolute error (*MAE*, %), root mean square error (*RMSE*), the coefficient of determination ($R^2$) and Nash-Sutcliffe model efficiency (*NSE*) statistical parameters calculated by the following Eqs. (6)–(9) were used to evaluate the regression results. The modelling dataset and the measured dataset is the same. All statistical analyses and figures were conducted in SPSS 18.0 and origin 2020.

$$MAE = \frac{1}{n}\sum_{i=1}^{n}\left|\frac{O_i - P_i}{O_i}\right| \quad (6)$$

$$RMSE = \sqrt{\frac{\sum_{i=1}^{n}(O_i - P_i)^2}{n-1}} \quad (7)$$

$$R^2 = \frac{\left[\sum_{i=1}^{n}\left(O_i - \overline{O}\right)\left(P_i - \overline{P}\right)\right]^2}{\sum_{i=1}^{n}\left(O_i - \overline{O}\right)^2 \sum_{i=1}^{n}\left(P_i - \overline{P}\right)^2} \quad (8)$$

$$NSE = 1 - \frac{\sum_{i=1}^{n}(O_i - P_i)^2}{\sum_{i=1}^{n}\left(O_i - \overline{O}\right)^2} \quad (9)$$

where $O_i$ is an observed value, $P_i$ is the predicted value, $\bar{O}$ is the mean observed value, $\overline{P}$ is the mean predicted value and $n$ is the number of samples.

## 3. Results and discussion

### 3.1. Differences in soil detachment capacity by rill flow among the soils

Statistics for soil detachment capacity of YL clay loess, CW loess, AS loess, DB sandy loess and SM sandy loess under the different combinations of slope and flow discharge are shown in Table 2. SM sandy loess had the largest $D_c$ with a mean of 2.2145 kg m$^{-2}$ s$^{-1}$, followed by YL clay loess, DB sandy loess, AS loess, and CW loess. The mean $D_c$ of SM sandy loess soil is 1.2, 2.4, 2.0 and 1.4 times that of YL clay loess, CW loess, AS loess, and DB sandy loess, respectively. One-way analysis of soil detachment capacity for the five loess soils was carried out (Fig. 4). The $D_c$ of YL clay loess is significantly different from CW loess and AS loess, but not significantly different from DB sandy loess or SM sandy loess. There was no significant difference between the $D_c$ of CW loess and AS loess, but there were significant differences between the $D_c$ of those soils and the $D_c$ of DB and SM sandy loess. Soil type influenced soil detachment capacity significantly.

The largest soil detachment capacity occurred in the SM sandy loess (Table 2 and Fig. 4), which is a sandy loam soil texture according to the USDA classification. Benaud et al. (2020) similarly found that the highest erosion rate (91.7 t ha$^{-1}$ yr$^{-1}$) was found on a medium sandy loam soil, demonstrating that excessively high soil loss rates can occur on light soils under arable land use. YL clay loess and DB and SM sandy loess belong to different loess zones, and the mechanical composition of YL clay loess and sandy loess have great differences, the clay content of YL clay loess is 3 ~ 5 times as much as DB and SM sandy loess. However, there was no significant difference between $D_c$ of YL clay loess and $D_c$ of sandy loess. This may be because YL clay loess soil aggregates well, but the poor bond between aggregates results in soil that is easily detached from the soil matrix, eventually leading to the YL clay loess having a large detachment capacity close to that of sandy loess.

**Table 2**
The statistic value of soil detachment capacity by rill flow for different soils.

| Soil | Minimum kg m$^{-2}$ s$^{-1}$ | Maximum kg m$^{-2}$ s$^{-1}$ | Meankg m$^{-2}$ s$^{-1}$ | $n$ |
|---|---|---|---|---|
| YL clay loess | 0.6243 | 3.9707 | 1.9320 | 25 |
| CW loess | 0.2800 | 2.0000 | 0.9435 | 25 |
| AS loess | 0.2654 | 2.3399 | 1.1189 | 25 |
| DB sandy loess | 0.4954 | 3.0488 | 1.6093 | 25 |
| SM sandy loess | 0.5571 | 4.0975 | 2.2154 | 25 |

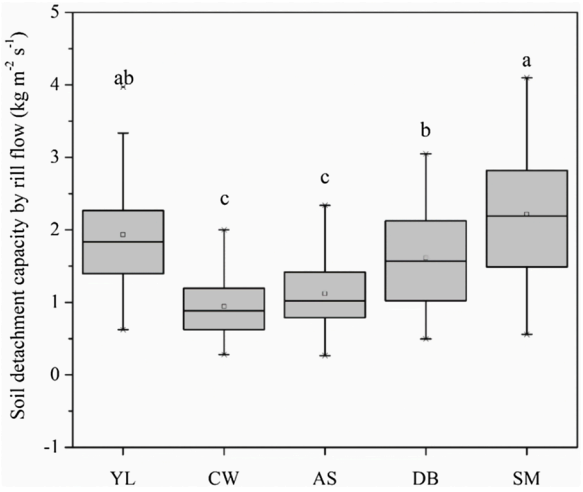


**Fig. 4.** Difference among soil detachment capacity by rill flow for the five loess soils (YL: YL clay loess; CW: CW loess; AS: AS loess; DB: DB sandy loess; SM: SM sandy loess).

### 3.2. Relationship between soil detachment capacity by rill flow and hydrodynamic parameters

The relationship between soil detachment capacity by rill flow ($D_c$) and corresponding flow shear stress ($\tau$) for the test soils was plotted in Fig. 5. It is obvious that $D_c$ increased as a linear function of shear stress for the five loess soils. The determination coefficients of the linear regression equation were between 0.93−0.98, showing good correlation with highly significant significance. Similar results were found in the relationship between $D_c$ and stream power ($w$) with coefficients of determination between 0.95−0.98 (Fig. 6). Soil detachment capacities also increased as unit stream power increased, and the relationship can be described by a power function (Fig. 7). As shown in Table 3, all of the regression equations had a significance level of $P < 0.01$, however, the error evaluation of the determination coefficient ($R^2$), Nash model efficiency coefficient (*NSE*), mean absolute error (*MAE*, %), and root mean square error (*RSME*) indicate that stream power is the best hydrodynamic parameter to describe the dynamic process of soil detachment capacity by rill flow for the five types of loess soil. The dynamic equation of the five soils is a linear equation between soil detachment capacity by rill flow and stream power ($R^2$: 0.95~0.98, $P$ <0.01).

The superiority of stream power in simulating the soil detachment process has being confirmed by Xiao et al. (2017); Zhang et al. (2015); Su et al. (2014); Zhang et al. (2003); Nearing et al. (1999), and Elliot and Laflen (1993). Although the test conditions in those studies differed, the variations only led to differences in equation type and coefficient, but does not change the conclusion that steam power is the optimal parameter for simulating the soil detachment capacity of rill flow.

### 3.3. Relationship between soil detachment capacity by rill flow and soil properties

Pearson correlation analysis was used to investigate the relationship between $D_c$ of the 5 test soils and soil properties (Table 4). The results show that soil detachment capacity by rill flow was negatively correlated with soil cohesion and effective silt content ($P < 0.05$), while it was positively correlated with effective median soil particle size ($P < 0.01$) and effective sand content ($P < 0.05$). The coefficients of correlation were 0.978, 0.900, 0.951 and 0.915, respectively. No statistically significant relationships were found between soil detachment capacity by rill flow and soil bulk density, organic matter, calcium carbonate content, cation substitution, or ultimate soil particle size.

Soil cohesion is a soil characteristic which can reflect the shear

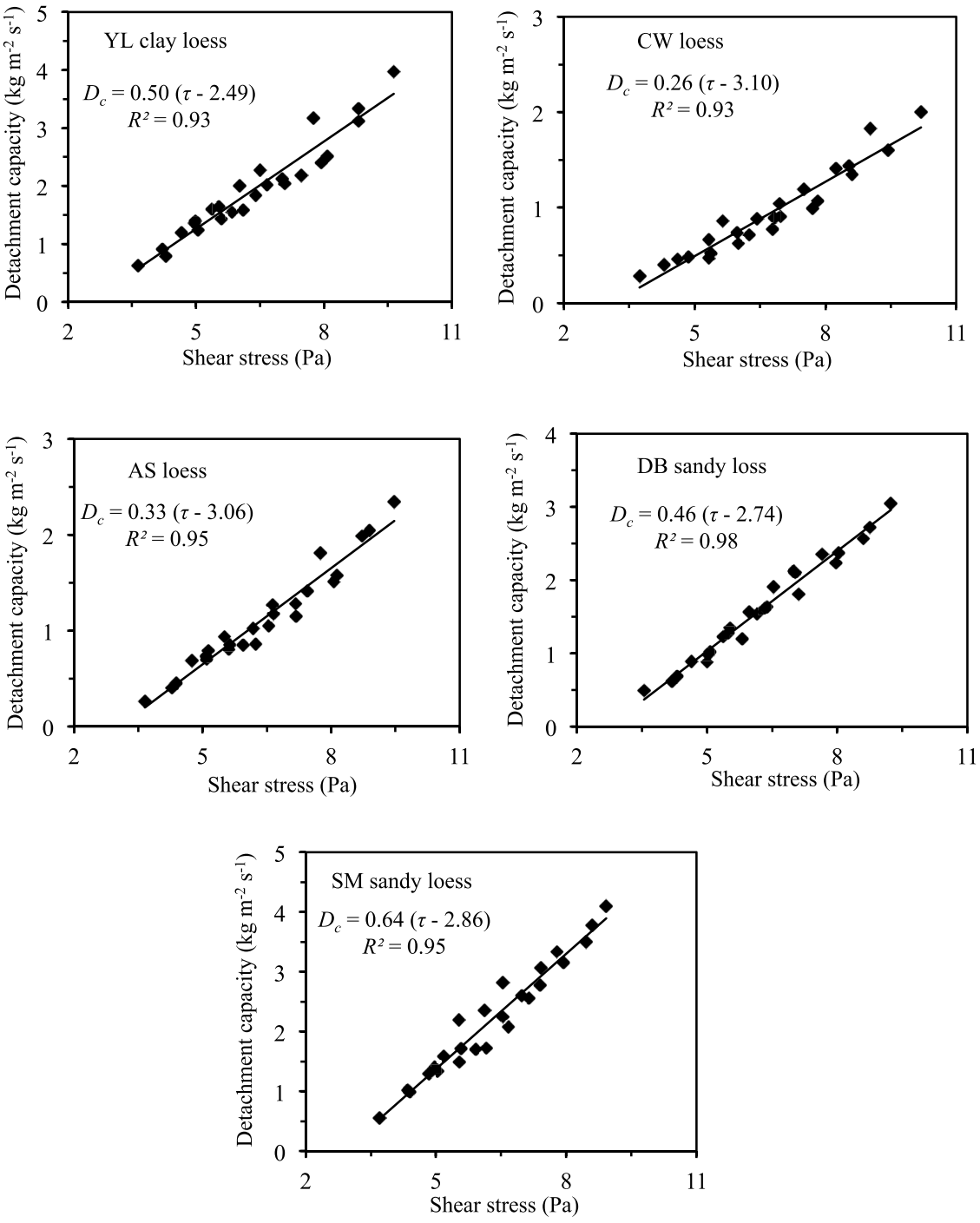


**Fig. 5.** Variation of soil detachment capacity by rill flow ($D_c$) with flow shear stress for the five loess soils.

strength of the soil. The greater the soil cohesion, the stronger the ability of soil particles to resist rill flow that would detach them from the soil mass, thus leading to decreased soil detachment capacity by rill flow. Therefore, there is a negative correlation between soil detachment capacity and soil cohesion, which was also confirmed by Zhang et al. (2008); Li et al. (2015a), and Geng et al. (2021).

In this study, soil detachment capacity by rill flow was correlated with the effective median particle size, the effective silt content and the effective sand content. These indexes were measured without any chemical dispersion and thus truly reflect soil particle size during actual erosion. Meanwhile, this study also reported that soil detachment capacity by rill flow had no correlation with ultimate soil particle size, which is the single grain distribution of soil particles after treatment with a chemical dispersant. Fig. 3 illustrates the particle size distribution of the five loess soils which was dispersed and undispersed. The cumulative percentage of YL clay loess and CW loess have large differences between the undispersed and dispersed treatments, which may lead to good correlation between $D_c$ and effective soil particle size, while the correlation between $D_c$ and ultimate soil particle size may be irrelevant. In addition, effective soil particle size distributions without any dispersion have an important influence on the soil detachment capacity by rill flow. However, the effective soil particle size distributions have rarely been used to study the relationship between soil detachment capacity and soil properties in previous studies. Our study shows that

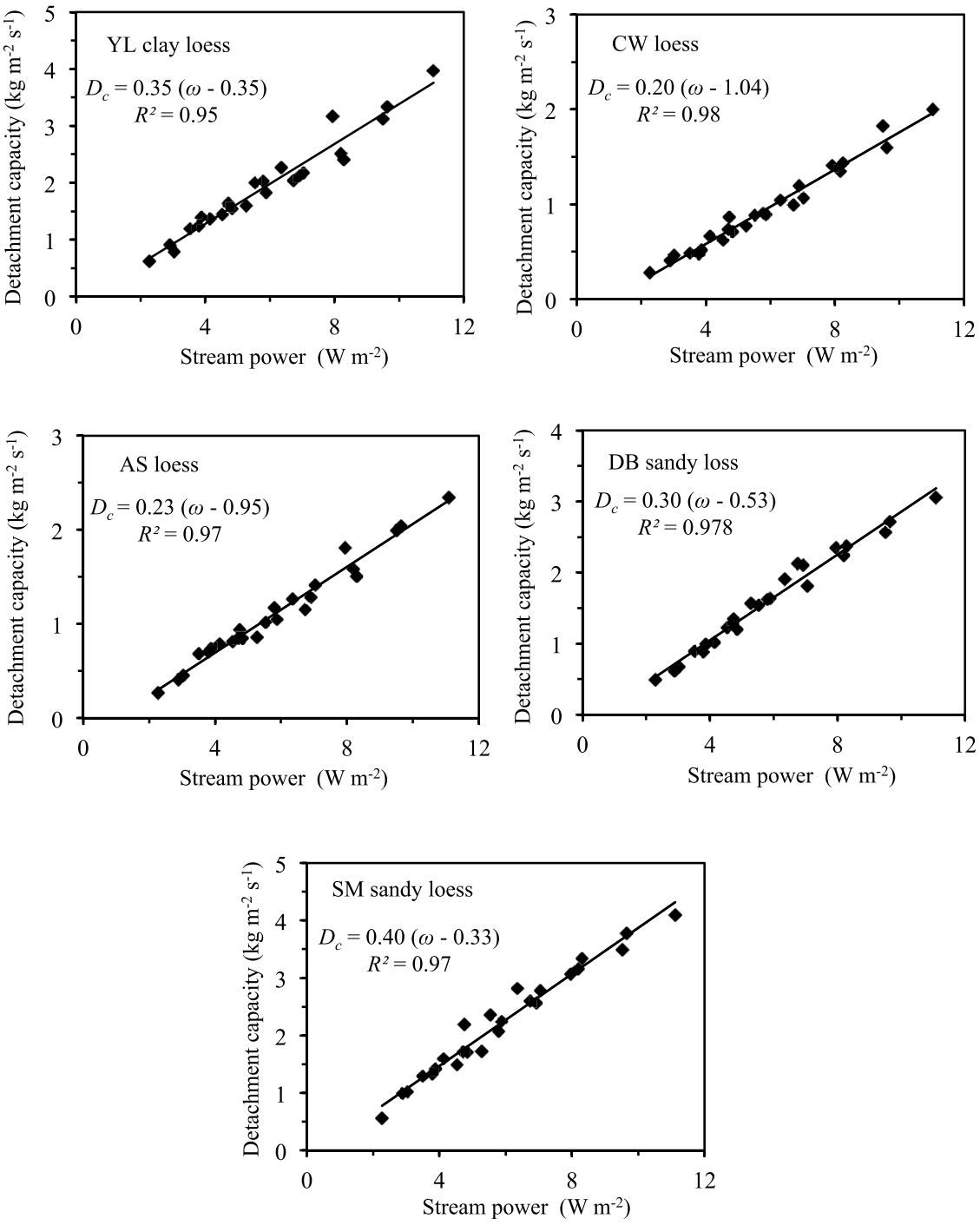


**Fig. 6.** Variation of soil detachment capacity by rill flow with stream power for the five loess soils.

attention should be paid to effective particle size distributions in which dispersion treatment is not applied in future studies, especially for soils with a large difference in cumulative percentage of soil particle size before and after dispersal.

Zhang et al. (2008), in a study on soil detachment capacity under different land use types in the Loess Plateau region, indicated that $D_c$ could be well simulated by the soil properties of clay content, bulk density, aggregate median diameter, and soil strength. Geng et al. (2015) studied the spatial variation of soil erodibility, and found that detachment capacity was negatively correlated with soil cohesion and silt content, and positively correlated with sand content. However, that study also showed that the effect of soil median particle size on the detachment capacity was not significant. Li et al. (2015b) looked at spatial variability in soil detachment capacity on a hillslope with an ephemeral gully and showed that $D_c$, soil cohesion, and clay content have a significant negative correlation, and that the median particle size of the soil and sand content were significantly positive correlated to $D_c$. Some of their results do not agree with the results of this study, however the differences may be because of differences in soil type, or may be due to whether the soil samples were treated with dispersant or not. There have been limited studies regarding soil samples without dispersion, thus perhaps explaining differing conclusions on the relationship between detachment capacity and soil particles.

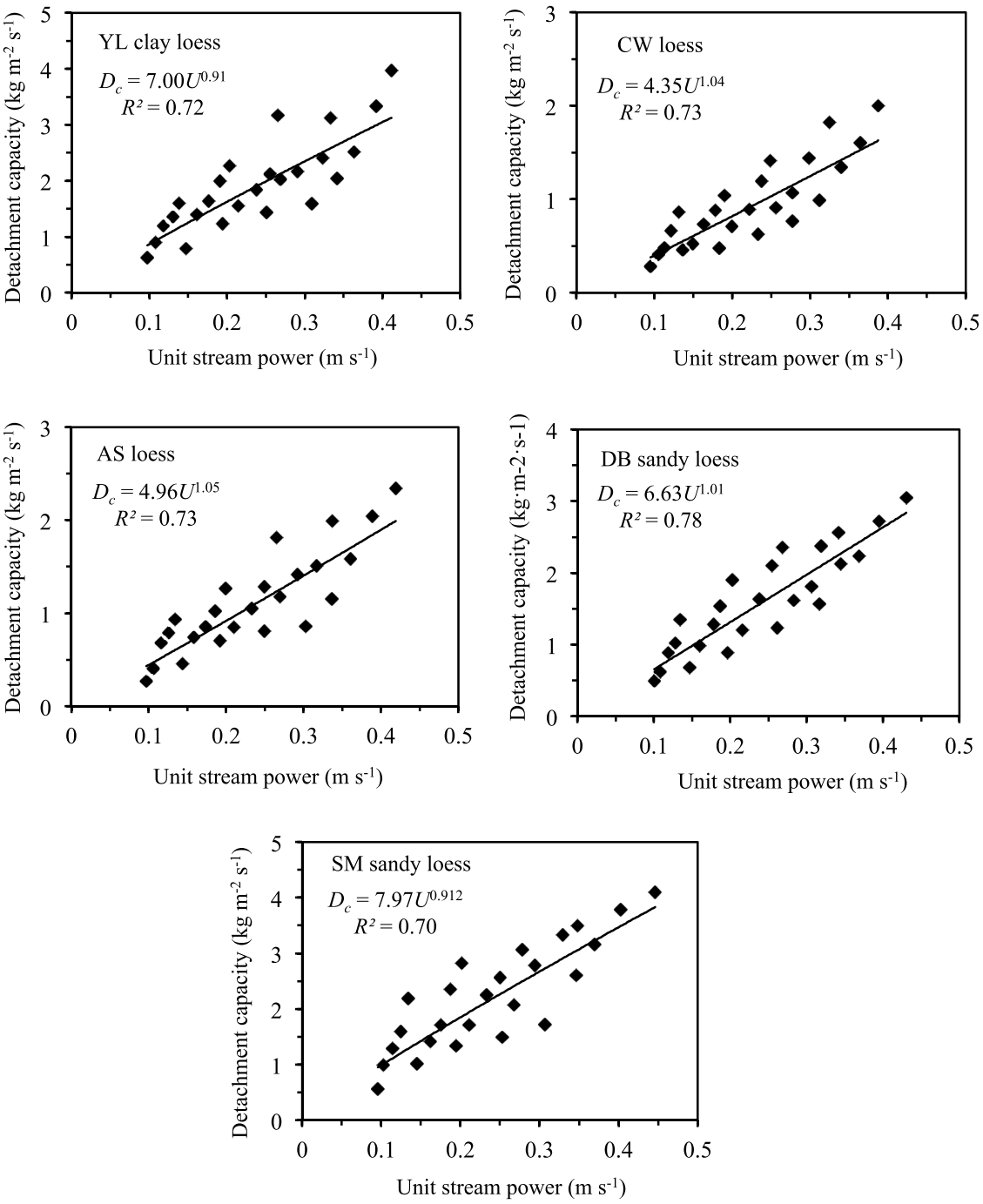


**Fig. 7.** Variation of soil detachment capacity by rill flow with unit stream power for the five loess soils.

### *3.4. Modelling soil detachment capacity by rill flow in the loess region*

Soil detachment capacity by rill flow is influenced significantly by hydraulic characteristics of rill flow and soil properties. Slope gradient and flow discharge are important conditions that determine the hydraulic characteristics of rill flow, but fortunately they are the most easily obtained hydraulic parameters. It is both feasible and practical to introduce slope gradient and flow discharge when simulating soil detachment capacity by rill flow. Slope gradient, flow discharge, soil cohesion and effective median particle size, which were proven to be most closely correlated with $D_c$ in the previous subsection were selected as factors to model soil detachment capacity by rill flow. Multivariate nonlinear regression analysis for the $D_c$ of the five loess soils showed that soil detachment capacity by rill flow could be modeled by a quaternary power function of slope gradient, flow discharges, soil cohesion and effective median particle size, as Eq. (10) shows.

$$D_c = 127.46\, S^{1.05}\, Q^{1.25}\, CH^{-1.13}\, D_{50}^{0.41} \quad (10)$$

($R^2 = 0.97$, $P < 0.01$, $NSE = 0.96$, $MAE = 7.13$ %, $RMSE = 0.17$, $n = 125$)

where $D_c$ is soil detachment capacity by rill flow (kg m$^{-2}$ s$^{-1}$); $S$ is slope gradient (%); $Q$ is unit flow discharge (m$^2$ s$^{-1}$); $CH$ is soil cohesion (kPa); $D_{50}$ is effective median particle size (μm).

The Nash model efficiency coefficient of Eq. (10) is 0.96. The mean absolute error (*MAE*) and root mean square error (*RMSE*) were 7.13 % and 0.17, respectively. The predicted value of $D_c$ calculated by Eq. (10) and the measured value of $D_c$ from the flume experiment were visualized

**Table 3**
Error evaluation of the relationship between soil detachment capacity by rill flow (kg $m^{-2}$ $s^{-1}$) and hydrodynamic parameters for different soils.

| Hydrodynamic parameter | Soil | Regression equation | $R^2$ | $P$ | $NSE$ | $MAE$ | $RMSE$ | $n$ |
|---|---|---|---|---|---|---|---|---|
| $\tau$ | YL clay loess | $D_c = 0.50(\tau - 2.49)$ | 0.93 | <0.01 | 0.93 | 9.30 | 0.22 | 25 |
| | CW loess | $D_c = 0.26(\tau - 3.10)$ | 0.93 | <0.01 | 0.98 | 12.96 | 0.12 | 25 |
| | AS loess | $D_c = 0.33(\tau - 3.06)$ | 0.95 | <0.01 | 0.97 | 9.11 | 0.12 | 25 |
| | DB sandy loess | $D_c = 0.46(\tau - 2.74)$ | 0.98 | <0.01 | 0.98 | 6.38 | 0.11 | 25 |
| | SM sandy loess | $D_c = 0.64(\tau - 2.86)$ | 0.95 | <0.01 | 0.97 | 7.71 | 0.22 | 25 |
| $\omega$ | YL clay loess | $D_c = 0.35(\omega - 0.35)$ | 0.95 | <0.01 | 0.95 | 7.21 | 0.18 | 25 |
| | CW loess | $D_c = 0.20(\omega - 1.03)$ | 0.98 | <0.01 | 0.98 | 6.80 | 0.070 | 25 |
| | AS loess | $D_c = 0.23(\omega - 0.95)$ | 0.97 | <0.01 | 0.97 | 6.82 | 0.09 | 25 |
| | DB sandy loess | $D_c = 0.30(\omega - 0.53)$ | 0.97 | <0.01 | 0.98 | 5.72 | 0.10 | 25 |
| | SM sandy loess | $D_c = 0.40(\omega - 0.33)$ | 0.97 | <0.01 | 0.97 | 6.85 | 0.17 | 25 |
| $U$ | YL clay loess | $D_c = 7.00U^{0.91}$ | 0.72 | <0.01 | 0.69 | 19.83 | 0.46 | 25 |
| | CW loess | $D_c = 4.35U^{1.04}$ | 0.73 | <0.01 | 0.73 | 21.89 | 0.24 | 25 |
| | AS loess | $D_c = 4.96U^{1.05}$ | 0.73 | <0.01 | 0.74 | 22.29 | 0.27 | 25 |
| | DB sandy loess | $D_c = 6.63U^{1.07}$ | 0.78 | <0.01 | 0.79 | 19.26 | 0.32 | 25 |
| | SM sandy loess | $D_c = 7.97U^{0.91}$ | 0.69 | <0.01 | 0.72 | 21.49 | 0.49 | 25 |

where $D_c$ is soil detachment capacity by rill flow (kg $m^{-2}$ $s^{-1}$); $\tau$ is shear stress (Pa); $\omega$ is stream power (W $m^{-2}$); $U$ is unit stream power (m $s^{-1}$); $R^2$ is determination coefficient; $P$ is significance level; $NSE$ is Nash-Sutcliffe model efficiency; $MAE$ mean absolute error (%); $RMSE$ root mean square error; $n$ is sample size.

**Table 4**
Pearson correlation coefficient matrix between soil detachment capacity by rill flow and soil properties among different soils.

| | | $D_c$ | γ | $OM$ | $CaCO_3$ | $PH$值 | $CEC$ | $CH$ | Effective particle size | | | | Ultimate particle size | | | |
|---|---|---|---|---|---|---|---|---|---|---|---|---|---|---|---|---|
| | | | | | | | | | $D_{50}$ | Clay | Silt | Sand | $D_{50}$ | Clay | Silt | Sand |
| $D_c$ | | 1 | | | | | | | | | | | | | | |
| γ | | .834 | 1 | | | | | | | | | | | | | |
| $OM$ | | −.302 | −.199 | 1 | | | | | | | | | | | | |
| $CaCO_3$ | | −.538 | −.529 | .934* | 1 | | | | | | | | | | | |
| $PH$值 | | .014 | .007 | −.918* | −.820 | 1 | | | | | | | | | | |
| $CEC$ | | −.746 | −.600 | .771 | .890* | −.653 | 1 | | | | | | | | | |
| $CH$ | | −.978** | −.757 | .461 | .657 | −.191 | .851 | 1 | | | | | | | | |
| Effective particle size | $D_{50}$ | .951* | .890* | −.032 | −.331 | −.223 | −.569 | −.873 | 1 | | | | | | | |
| | Clay | −.811 | −.961** | .392 | .670 | −.155 | .639 | .760 | −.805 | 1 | | | | | | |
| | Silt | −.900* | −.895* | .022 | .342 | .149 | .612 | .831 | −.969** | .769 | 1 | | | | | |
| | Sand | .915* | .935* | −.083 | −.407 | −.104 | −.636 | −.846 | .974** | −.831 | −.995** | 1 | | | | |
| Ultimate particle size | $D_{50}$ | .370 | .336 | −.960** | −.965** | .932* | −.865 | −.519 | .141 | −.468 | −.191 | .243 | 1 | | | |
| | Clay | −.138 | −.108 | .962** | .887* | −.990** | .725 | .308 | .110 | .267 | −.058 | .007 | −.968** | 1 | | |
| | Silt | −.495 | −.455 | .924* | .976** | −.871 | .927* | .629 | −.285 | .562 | .337 | −.385 | −.988** | .920* | 1 | |
| | Sand | .368 | .331 | −.957* | −.961** | .933* | −.868 | −.519 | .139 | −.460 | −.193 | .243 | 1.000** | −.968** | −.989** | 1 |

** Significant at $P < 0.01$.
* Significant at $P < 0.05$; $D_c$: soil detachment capacity by rill flow (kg $m^{-2}$ $s^{-1}$); γ: soil bulk density (g $cm^{-3}$); $OM$: organic matter content (g $kg^{-1}$); $CaCO_3$: calcium carbonate content (g kg); $pH$ : $pH$ value; $CEC$: cation substitution amount (cmol $kg^{-1}$) ; $CH$: soil cohesion (kPa) ; $D_{50}$: median particle size (μm); Clay: clay content (%); Silt: silt content (%); Sand: sand content (%).

in the Cartesian coordinate system (Fig. 8A). The predicted and measured $D_c$ is distributed closely around the 1:1 line, which illustrates that the simulation accuracy of Eq. (10) for soil detachment capacity is high. However, the data point distribution is more scattered when $D_c$ is greater than 3 kg $m^{-2}$ $s^{-1}$ which illustrates a relatively low simulation precision when the $D_c$ value is greater than 3 kg $m^{-2}$ $s^{-1}$. All the indexes illustrate that Eq. (10) predicts soil detachment capacity well and can be used to calculate soil detachment capacity by rill flow for different hydraulic and soil conditions in the loess region.

Stream power, which proved to be the best hydrodynamic parameter for estimating $D_c$, and soil cohesion and effective median particle size, which were the soil properties most closely correlation with $D_c$, were selected as factors to model soil detachment capacity by rill flow. Multivariate nonlinear regression analysis for $D_c$ of the five loess soils shows that soil detachment capacity by rill flow could be modeled by a ternary power function which indicates variation in soil detachment capacity by stream power, soil cohesion and effective median size, as illustrated in Eq. (11),

$$D_c = 0.26\ \omega^{1.18}\ CH^{-1.12}\ D_{50}^{0.42} \quad (11)$$

($R^2 = 0.97$, $P < 0.01$, $NSE = 0.96$, $MAE = 8.02$ %, $RMSE = 0.18$, $n = 125$)

where $D_c$ is soil detachment capacity by rill flow (kg $m^{-2}$ $s^{-1}$); $w$ is stream power (W $m^{-2}$); $CH$ is soil cohesion (kPa); $D_{50}$ is effective median particle size (μm).

The $NSE$ of Eq. (11) is 0.96, while the $MAE$ and $RMSE$ were 8.02 % and 0.18, respectively. All of the error indexes agree that Eq. (11) predicts soil detachment capacity well. The predicted value of soil detachment capacity by rill flow calculated using Eq. (11) and the measured values from the flume experiment were distributed around the 1:1 line (Fig. 8B), and the simulation accuracy of Eq. (11) for soil detachment capacity by rill flow is high. Eq. (11) can be used to calculate soil detachment capacity by rill flow for various hydraulic and soil conditions in the loess region.

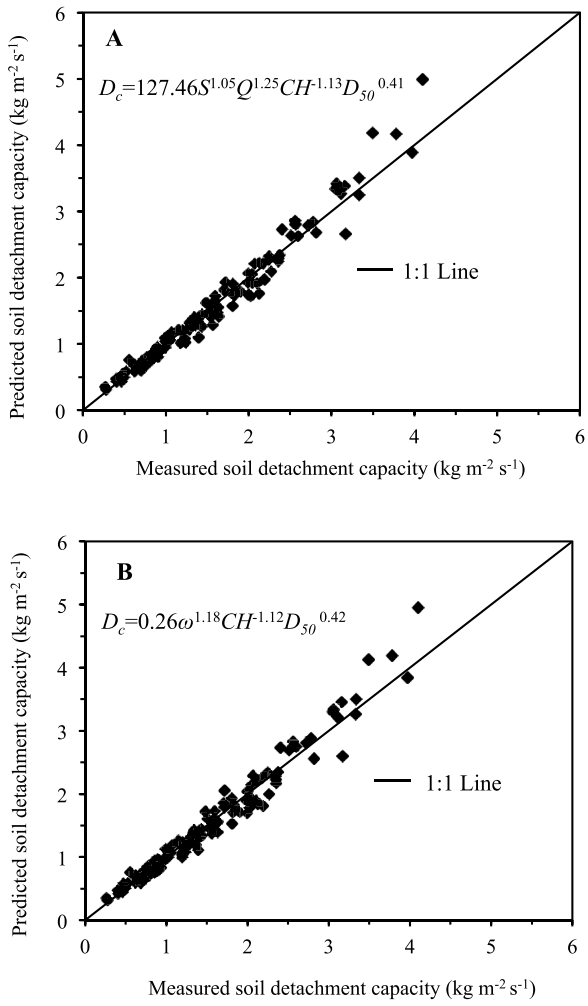


**Fig. 8.** Measured vs. predicted soil detachment capacity by rill flow using the established Eq. (10) and (11).

## 4. Conclusion

Soil detachment capacity by rill flow for five typical loess soils on the Loess Plateau of China was investigated through a flume experiment, and testing of soil physical and chemical properties. SM sandy loess had the largest $D_c$ with a mean of 2.2145 kg m$^{-2}$ s$^{-1}$, followed by YL clay loess, DB sandy loess, AS loess, and CW loess. $D_c$ of YL clay loess significantly differed from that of CW loess and AS loess, but not from DB sandy loess and SM sandy loess. A high erosion rate occurred on sandy loam compared to loam, silty loam, and silty clay loam soils. Stream power was the best hydrodynamic parameter to describe the dynamic process of soil detachment capacity by rill flow for the five loess soils. The dynamic equation for the five soils is a linear equation between soil detachment capacity by rill flow and stream power ($R^2$: 0.96~0.98, $P <$ 0.01). Soil detachment capacity by rill flow was negatively correlated with soil cohesion and effective silt content ($P < 0.05$), while it was positively correlated with effective median soil particle size ($P < 0.01$) and effective sand content ($P < 0.05$). None of the indexes for ultimate particle size had a statistical significant relationship with $D_c$. Two equations were established to model soil detachment capacity by rill flow for various hydraulic and soil conditions in the loess region. Soil detachment capacity by rill flow could be modeled by a quaternary power function of slope gradient, flow discharge, soil cohesion and effective median particle size ($R^2 = 0.97$; $NSE = 0.96$ ; $P < 0.01$), or by a ternary power function which calculates the variation in soil detachment capacity with stream power, soil cohesion and effective median particle size ($R^2 = 0.97$; $NSE = 0.96$; $P<0.01$).

The results of this study are helpful for revealing the mechanism of soil detachment by rill flow and accurately estimating soil detachment capacity by rill flow on the Loess Plateau. And to this end, we also note that there is a real need to introduce both effective and ultimate particle sizes in future studies of rill erosion, especially for soils in which there are large differences in particle size distribution before and after chemical dispersal, to ensure full, systematic understanding of soil erosion processes. Initial soil moisture conditions, soil bulk density, and soil frost-heave are important field condition factors that could influence the rill erosion process but were not investigated in this laboratory study, which are limitations of this study. These factors will be considered in the future study, in which soil detachment capacity under different initial soil moistures, vegetation, bulk densities, and temperatures will be investigated.

## Declaration of Competing Interest

The authors report no declarations of interest.

## Acknowledgements

Financial support for this research was provided by the National Natural Science Foundation of China funded project (41907054; 41830758; 41867015); the National Key Research and Development Program of China (2017YFD0800502); the Chinese Universities Scientific Fund (2452020205); the State Key Laboratory of Soil Erosion and Dryland Farming on the Loess Plateau (A314021402-2001).

## References

Benaud, P., Anderson, K., Evans, M., Farrow, L., Glendell, M., James, M.R., et al., 2020. National-scale geodata describe widespread accelerated soil erosion. Geoderma 371 doi: ARTN 11437810.1016/j.geoderma.2020.114378.
Cao, L.X., Zhang, K.L., Dai, H.L., Guo, Z.L., 2011. Modeling soil detachment on unpaved road surfaces on the Loess Plateau. Trans. Asabe 54 (4), 1377–1384.
Ciampalini, R., Torri, D., 1998. Detachment of soil particles by shallow flow: sampling methodology and observations. Catena 32 (1), 37–53.
Cochrane, T.A., Flanagan, D.C., 1997. Detachment in a simulated rill. Trans. Asae 40 (1), 111–119.
De Baets, S., Poesen, J., 2010. Empirical models for predicting the erosion-reducing effects of plant roots during concentrated flow erosion. Geomorphology 118, 425–432.
De Baets, S., Poesen, J., Gyssels, G., Knapen, A., 2006. Effects of grass roots on the erodibility of topsoils during concentrated flow. Geomorphology 76, 54–67.
De Roo, A.P.J., Wesseling, C.G., Ritsema, C.J., 1996. LISEM: a single-event physically based hydrological and soil erosion model for drainage basins. I: theory, input and output. Hydrol. Process. 10 (8), 1107–1117.
Elliot, W.J., Laflen, J.M., 1993. A process -based rill erosion model. Trans. ASAE 36 (1), 65–72.
Flangan, D.C., Nearing, M.A., 1995. USDA Water Erosion Prediction Project: Hillslope Profile and Watershed Model Documentation. USDA - Agricultural Research Service, NSERL Report No. 10, West Lafayette, 47907-1196.
Foster, G.R., Huggins, L.F., Meyer, L.D., 1984. A laboratory study of rill hydraulics. II. Shear stress relationships. Trans. ASAE 27 (3), 797–804. https://doi.org/10.13031/2013.32874.
Geng, R., Zhang, G.H., Li, Z.W., Wang, H., 2015. Spatial variation in soil resistance to flowing water erosion along a regional transect in the Loess Plateau. Earth Surf. Process. Landf. 40 (15), 2049–2058. https://doi.org/10.1002/esp.3779.
Geng, R., Zhang, G.H., Hong, D.L., Ma, Q.H., Shi, Y.Z., 2021. Response of soil detachment capacity to landscape positions in hilly and gully regions of the loess plateau. Catena 196, 104852.
Ghebreiyessus, Y.T., Gantzer, C.J., Alberts, E.E., Lentz, R.W., 1994. Soil erosion by concentration flow: shear stress and bulk density. Trans. ASAE 37 (6), 1791–1797.
Gimenez, R., Govers, G., 2002. Flow detachment by concentrated flow on smooth and irregular beds. Soil Sci. Soc. Am. J. 66 (5), 1475–1483.
Gover, G., 1992. Evaluation of transport capacity formula for overland flow. In: Parsons, A.J., Abrahams, A.D. (Eds.), Overland Flow: Hydraulics and Erosion Mechanics. UCL Press, London, pp. 243–273.
Govers, G., 1990. Empirical relationships for the transport formulae of overland flow. In: Erosion, Transport and Deposition Processes(Proceedings of the Jerusalem Workshop, March-April 1987). IAHS (International Association of Hydrological Sciences), pp. 45–63. Publication no. 189.
Govers, G., Gimenez, R., Oost, K.V., 2007. Rill erosion: exploring the relationship between experiments, modeling and field observation. Earth. Rev. 84 (3–4), 87–102.
Horton, R.E., Leach, H.R., Vliet, R.V., 1934. Laminar Sheet Flow. Transactions of the American Geophysical Union, pp. 393–404.

Knapen, A., Poesen, J., Govers, G., Gyssels, G., Nachtergaele, J., 2007. Resistance of soils to concentrated flow erosion: a review. Earth Science Reviews 80, 75–109.
Li, Z.W., Zhang, G.H., Geng, R., Wang, H., Zhang, X.C., 2015a. Land use impacts on soil detachment capacity by overland flow in the Loess Plateau. China. Catena 124, 9–17. https://doi.org/10.1016/j.catena.2014.08.019.
Li, Z.W., Zhang, G.H., Geng, R., Wang, H., 2015b. Spatial heterogeneity of soil detachment capacity by overland flow at a hillslope with ephemeral gullies on the Loess Plateau. Geomorphology 248, 264–272. https://doi.org/10.1016/j.geomorph.2015.07.036.
Liu, D.S., 1966. Material Composition and Structure of Loess. Science Press, pp. P2–P4.
Liu, F., Zhang, G.H., Sun, L., Wang, H., 2016. Effects of biological soil crusts on soil detachment process by overland flow in the Loess Plateau of China. Earth Surf. Process. Landf. 41 (7), 875–883. https://doi.org/10.1002/esp.3870.
Liu, Je., Zhang, X., Zhou, Z., 2019. Quantifying effects of root systems of planted and natural vegetation on rill detachment and erodibility of a loessial soil. Soil Tillage Res. 195, 104420 https://doi.org/10.1016/j.still.2019.104420.
Luk, S.H., Merz, W., 1992. Use of the salt tracing technique to determine the velocity of overland flow. Soil Technol. 5, 289–301.
Mamo, M., Bubenzer, G.D., 2001. Detachment rate, soil erodibility, and soil strength as influenced by living plant roots part I: laboratory study. Trans. Asae 44 (5), 1167–1174.
Misra, R.K., Rose, C.W., 1996. Application and sensitivity analysis of process-based erosion model GUEST. Eur. J. Soil Sci. 47 (4), 593–604.
Morgan, R.P.C., Quinton, J.N., Smith, R.E., Govers, G., Poesen, J.W.A., Auerswald, K., Chisci, G., Torri, D., Styczen, M.E., 1998. The European Soil Erosion model (EUROSEM): a dynamic approach for predicting sediment transport from fields and small catchments. Earth Surface Process and Landforms 23 (6), 527–544.
Nearing, M.A., 1997. The mechanics of soil detachment by raindrops and runoff. Eurasian Soil Sci. 30 (5), 552–556.
Nearing, M.A., Bradford, J.M., Parker, S.C., 1991. Soil detachment by shallow flow at low slopes. Soil Sci. Soc. Am. J. 55 (2), 339–344.
Nearing, M.A., Simanton, J.R., Norton, L.D., Bulygin, S.J., Stone, J., 1999. Soil erosion by surface water flow on a stony, semiarid hillslope. Earth Surf. Process. Landf. 8 (24), 677–686.
Su, Z.L., Zhang, G.H., Yi, T., Liu, F., 2014. Soil detachment capacity by overland flow for soils of the Beijing Region. Soil Sci. 179 (9), 446–453. https://doi.org/10.1097/ss.0000000000000089.
Torri, D., Ciampalini, R., Accolti, G.P., 1998. The role of aggregates on soil erosion processes. In: Presented at the "Global Changes: Modeling Soil Erosion by Water" Conference. NATO ARW. Oxford, U.K., October 1995.
Wang, J.G., Li, Z.X., Cai, C.F., Yang, W., Ma, R.M., Zhang, G.B., 2012. Predicting physical equations of soil detachment by simulated concentrated flow in Ultisols (subtropical China). Earth Surf. Process. Landf. 37 (6), 633–641. https://doi.org/10.1002/esp.3195.
Wang, B., Zhang, G.H., Shi, Y.Y., Zhang, X.C., Ren, Z.P., Zhu, L.J., 2013. Effect of natural restoration time of abandoned farmland on soil detachment by overland flow in the Loess Plateau of China. Earth Surf. Process. Landf. 38 (14), 1725–1734. https://doi.org/10.1002/esp.3459.
Wang, B., Zhang, G.H., Shi, Y.Y., Li, Z.W., Shan, Z.J., 2015. Effects of near soil surface characteristics on the soil detachment process in a chronological series of vegetation restoration. Soil Sci. Soc. Am. J. 79 (4), 1213–1222. https://doi.org/10.2136/sssaj2015.03.0120.
Wang, D.D., Wang, Z.L., Shen, N., Chen, H., 2016. Modeling soil detachment capacity by rill flow using hydraulic parameters. J. Hydrol. 535, 473–479. https://doi.org/10.1016/j.jhydrol.2016.02.013.
Xiao, H., Liu, G., Liu, P.L., Zheng, F.L., Zhang, J.Q., Hu, F.N., 2017. Response of soil detachment rate to the hydraulic parameters of concentrated flow on steep loessial slopes on the Loess Plateau of China. Hydrol. Process. 31 (14), 2613–2621. https://doi.org/10.1002/hyp.11210.
Yang, C.T., 1972. Unit stream power and sediment transport. Journal of the Hydraulics Division 98 (10), 1805–1826.
Zhang, G.H., Liu, B.Y., Mearing, M.A., Huang, C.H., Zhang, K.L., 2002. Soil detachment by shallow flow. Trans. Asae 45 (2), 351–357.
Zhang, G.H., Liu, B.Y., Liu, G.B., He, X.W., Nearing, M.A., 2003. Detachment of undisturbed soil by shallow flow. Soil Sci. Soc. Am. J. 67 (3), 713–719.
Zhang, G.H., Liu, G.B., Tang, K.M., Zhang, X.C., 2008. Flow detachment of soils under different land uses in the Loess Plateau of China. Trans. Asabe 51 (3), 883–890.
Zhang, G.H., Liu, Y.M., Han, Y.F., Zhang, X.H., 2009. Sediment transport and soil detachment on steep slopes: I. Transport capacity estimation. Soil Sci. Soc. Am. J. 73 (4), 1291–1297.
Zhang, L.T., Gao, Z.L., Yang, S.W., Li, Y.H., Tian, H.W., 2015. Dynamic processes of soil erosion by runoff on engineered landforms derived from expressway construction: A case study of typical steep spoil heap. Catena 128, 108–121. https://doi.org/10.1016/j.catena.2015.01.020.
Zheng, F.L., Zhang, X.C., Wang, J.X., Flanagan, D.C., 2020. Assessing applicability of the WEPP hillslope model to steep landscapes in the northern Loess Plateau of China. Soil Tillage Res. 197 https://doi.org/10.1016/j.still.2019.104492, 104492.